PHYSICAL REVIEW B VOLUME 27, NUMBER 6 15 MARCH 1983

Photoemission spectra and band structures of d-band metals. X. Relativistic momentum matrix elements

R. L. Benbow*
Department of Physics, Northern Illinois University, Dekalb, Illinois 60115

N. V. Smith
Bell Laboratories, Murray Hill, New Jersey 07974
(Received 21 September 1982)

Band-structure calculations are performed to assess the magnitude of relativistic effects in angle-resolved photoemission. The specific case of normal emission from Ag(111) is considered using a combined interpolation scheme which incorporates spin-orbit coupling both within the d bands and between the plane waves of the basis set. Detailed numerical results are presented for the momentum matrix elements in the nonrelativistic and relativistic cases for all the initial-state bands in both parallel and perpendicular polarization. The observability of relativistic effects in available and future experimental data is discussed.

I. INTRODUCTION

The precision with which angle-resolved photoemission can determine band structures continues to grow, and it is now necessary to consider effects which have hitherto been regarded as negligible. Relativistic effects represent a case in point. For example, in Cu (not usually regarded as a relativistic metal) it is now possible to resolve the spin-orbit splitting in the d band.[1] Our concern in this paper will be with spin-orbit splitting, but more especially with the subtle ways in which relativistic effects influence the momentum matrix elements for optical transitions.

This paper is one in a series whose unifying theme is the use of a combined interpolation scheme to mediate between photoemission experiments and first-principles band calculations. Part of the work has consisted in refining the combined interpolation scheme itself. Paper I of the series[2] described certain improvements over the original schemes of Hodges *et al.*[3] and Mueller.[4] Paper VII extended the scheme to higher energies and reported successful attempts to compute the optical momentum matrix elements from derivatives of the Hamiltonian.[5] In this paper we extend the scheme further by inclusion of spin-orbit splitting in the unoccupied (i.e., plane-wave) bands. Taking the particular case of normal photoemission from Ag(111), we compute the momentum matrix elements and examine in detail the way in which relativistic selection rules lead to expectations different from those based on nonrelativistic selection rules. Our discussion here is timely since it has been suggested in the recent literature[6] that the lowering of symmetry associated with the inclusion of relativistic effects will lead to an abundance of new transitions which would have been symmetry-forbidden in the nonrelativistic case.

The format of this paper is as follows. Section II describes the formal inclusion of spin-orbit effects in the unoccupied bands and illustrates the results of fitting the scheme to the first-principles calculations on Ag. In Sec. III the computation of relativistic momentum matrix elements is discussed and comparisons are made with nonrelativistic Ag to show how inclusion of relativistic interactions affects the momentum matrix elements. Some of the motivation for this computational effort may be found in a subsequent paper,[7] where extensive experimental results on Ag(001) may be found. While we do make some contact with experiment in Sec. III, our main emphasis here is with the technicalities, magnitudes, and observability of relativistic effects in photoemission. The Appendix lists certain symmetrizing factors which are required in the successful operation of the interpolation scheme but which have not been described in previous papers of the series.

II. RELATIVISTIC INTERACTIONS AND THE BAND STRUCTURE OF Ag

Previous versions of the combined interpolation scheme have included spin-orbit splitting only in the d bands.[2,5,8] For completeness, we now include spin-orbit coupling between the plane-wave (PW) basis states of the scheme. We then recalculate the

bands of Ag so as to simulate the first-principles relativistic augmented plane-wave (APW) results of Christensen.[9] The relativistic changes to the band structure are quite appreciable. This sets the stage for our discussion in Sec. III of momentum matrix elements and relativistic selection rules.

A. Relativistic PW-PW interactions

The PW states of the interpolation scheme interact with each other through a pseudopotential which has local and nonlocal parts. The nonlocal part arises through orthogonalization to the d states and takes the form[2]

$$H_{\text{non}}=Sj_2(k_iR)j_2(k_jR)P_2(\hat{k}_i\cdot\hat{k}_j)\ . \tag{1}$$

Here $\vec{k}_i$ and $\vec{k}_j$ are wave vectors of the form $\vec{k}+\vec{G}_i$ and $\vec{k}+\vec{G}_j$, where $\vec{k}$ is the reduced wave vector and $\vec{G}_i$ and $\vec{G}_j$ are reciprocal-lattice vectors; j_2 and P_2 are the usual spherical Bessel function and Legendre polynomial of order 2; S and R are treated as disposable parameters. The success of this term in its ability to mimic the behavior of band gaps of first-principles calculations is attributed[2] to its strong similarity to the $l=2$ term in the standard APW Hamiltonian. In the relativistic APW formalism, there is an additional interaction between the PW's due to spin-orbit coupling which (following Christensen and Seraphin[10]) may be written,

$$H_{\text{s.o.}}=\frac{4\pi R_s^2}{\Omega_c}\sum_{l=1}^{\infty}P_l'(\hat{k}_i\cdot\hat{k}_j)j_l(k_iR_s)j_l(k_jR_s)\times\beta_l(E)\langle m_i\,|\,i\vec{\sigma}\cdot\vec{k}_j\times\vec{k}_i\,|\,m_j\rangle\ . \tag{2}$$

Here Ω_c is the volume of the unit cell, R_s is the muffin-tin radius, and $\beta_l(E)$ are energy-dependent spin-orbit parameters; j_l are again spherical Bessel functions of order l; $P_l'(\hat{k}_i\cdot\hat{k}_j)$ are the first derivative with respect to the argument of the Legendre polynomials of order l; $|m_i\rangle$ are the spin eigenstates of the ith electron states. It happens in our case that the complete expansion is unnecessary when we consider that we are dealing with only the $\vec{L}\cdot\vec{S}$ term in the Hamiltonian. This term is generally small in comparison with the kinetic energy, pseudopotential, and nonlocal terms in the free-electron part of the Hamiltonian. It is found that we may adopt the formulation of Cohen and Heine,[11] who have truncated (2) to be a first-order polynomial in $(\hat{k}_i\cdot\hat{k}_j)$:

$$H_{\text{s.o.}}=[\lambda_1+\lambda_2(\hat{k}_i\cdot\hat{k}_j)]\langle m_i\,|\,i\vec{\sigma}\cdot\vec{k}_j\times\vec{k}_i\,|\,m_j\rangle\ . \tag{3}$$

λ_1 and λ_2 are constants which we treat as disposable parameters to be chosen so as to give the proper splitting of certain PW bands. Noting that

$$\begin{aligned}&\langle\pm\tfrac{1}{2}\,|\,\vec{\sigma}\,|\,\pm\tfrac{1}{2}\rangle=\pm i\hat{z}\ ,\\&\langle\pm\tfrac{1}{2}\,|\,\vec{\sigma}\,|\,\mp\tfrac{1}{2}\rangle=\hat{x}\mp i\hat{y}\ ,\end{aligned} \tag{4}$$

we have the following explicit k-dependent forms

$$\begin{aligned}&\langle\pm\tfrac{1}{2}\,|\,i\vec{\sigma}\cdot\vec{k}_j\times\vec{k}_i\,|\,\pm\tfrac{1}{2}\rangle=\pm i(k_x^jk_y^i-k_y^jk_x^i)\ ,\\&\langle\pm\tfrac{1}{2}\,|\,i\vec{\sigma}\cdot\vec{k}_j\times\vec{k}_i\,|\,\mp\tfrac{1}{2}\rangle=i(k_y^jk_z^i-k_z^jk_y^i)\pm(k_z^jk_x^i-k_x^jk_z^i)\ .\end{aligned} \tag{5}$$

The complete Hamiltonian matrix, including both the PW and the d terms, is now

$$H=\begin{bmatrix}H_{cc}+H_{cc}^{++} & H_{cd} & H_{cc}^{+-} & 0\\ H_{dc} & H_{dd}+\xi H_{dd}^{++} & 0 & \xi H_{dd}^{+-}\\ H_{cc}^{-+} & 0 & H_{cc}+H_{cc}^{--} & H_{cd}\\ 0 & \xi H_{dd}^{-+} & H_{dc} & H_{dd}+\xi H_{dd}^{--}\end{bmatrix}\ . \tag{6}$$

H_{cc}, H_{cd} (or H_{dc}), and H_{dd} are, respectively, the 16×16 PW-PW, the 16×5 (or 5×16) PW-d, and 5×5 d-d interaction matrices for the combined interpolation scheme without spin-orbit effects. The $H_{dd}^{\pm\pm}$ are the 5×5 spin-orbit matrices of Abate and Asdente[12] added previously to the interpolation scheme. The $H_{cc}^{\pm\pm}$ are the 16×16 PW-PW matrices constructed from Eq. (3) using the explicit forms of Eq. (5).

Spin-orbit interactions must be included explicitly in the Hamiltonian since they bring about a qualitative change in the form of the bands. The other relativistic effects (mass velocity and Darwin shifts) can simply be absorbed into the existing parametrization of the scheme, as has been explained previously in Ref. 8.

B. Band structure of Ag

We have recomputed the band structure of Ag with the combined interpolation scheme

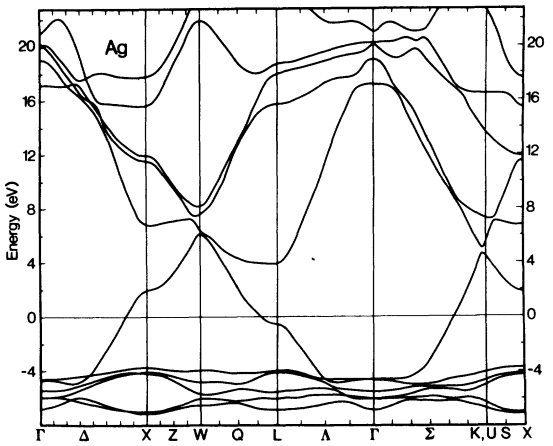

FIG. 1. Band structure of Ag obtained from the combined interpolation scheme with all relativistic interactions. The parameters (Table I) were arranged to reproduce the first-principles results of Christensen (Ref. 9).

parametrized to fit the first-principles calculations of Christensen.[9] The bands are shown in Fig. 1, and the parameters are listed in Table I. Inclusion of the additional PW-PW interaction has had the desired effect, viz., it has removed from the upper bands degeneracies left by the nonrelativistic interpolation scheme. It has also introduced a few relativistic gaps in the higher-lying bands, since bands of like symmetry are not allowed to touch (i.e., to cross).

TABLE I. Parameters of the combined interpolation scheme for Ag, arranged to reproduce the relativistic first-principles results of Christensen (Ref. 9). Energies are in rydbergs. The Fermi level is $E_F=0.444$ Ry.

d bands	
E	0.1070
Δ	−0.0039
A_1	0.011 14
A_2	0.002 15
A_3	0.005 47
A_4	0.006 63
A_5	0.001 64
A_6	0.004 39
Plane-wave bands	
α	0.010 50
V_{000}	−0.0378
V_{111}	0.0625
V_{200}	0.0484
V_{220}	−0.0010
V_{311}	0.0848
V_{222}	0.1243
Hybridization and orthogonalization	
R	0.294
B_t, B_e	1.442
S	1.480
Spin orbit	
ξ	0.0190
λ_1	0.000 05
λ_2	0.000 08

The energy eigenvalues tabulated by Christensen in Ref. 9 have been used in strict order. This leads us to bands which simulate those of Ref. 9 quite well. We find, however, that we differ with Christensen in the labeling and identification of some of the bands according to appropriate double-group representations. Specifically at L and along Λ in the Brillouin zone, Christensen labels band 2 as L_4^+ (or Λ_4) and band 3 as $L_5^+ + L_6^+$ (or $\Lambda_5+\Lambda_6$); we label them oppositely. Our calculated momentum matrix elements obey the correct relativistic selection rules, thus confirming our identifications. Note that Christensen also uses a convention for labeling the symmetry of the group C_{3v} (and C_3), which differs from that originally established by Elliott.[13] Elliott chose to label the twofold degenerate states as $L_6^{\pm}$ (Λ_6) and the time-reversal degenerate states as $L_4^{\pm}+L_5^{\pm}$ ($\Lambda_4+\Lambda_5$). We here use the convention of Elliott.[13] Thus band 2 at L is $L_4^+ + L_5^+$ and band 3 is labeled L_6^+ with corresponding changes along Λ. The influence of both PW-PW and d-d spin-orbit interaction is illustrated in Fig. 2 where we compare the bands along Λ for the relativistic and nonrelativistic cases.

III. RELATIVISTIC MOMENTUM MATRIX ELEMENTS

A. Basic expressions

In comparing the strengths of optical transitions we need to evaluate the matrix elements $\vec{\pi}_{fi}$ ($\equiv\langle f \mid \vec{\pi} \mid i\rangle$) of the operator,

$$\vec{\pi}=\vec{\mathrm{P}}+\frac{\hbar}{4mc^2}(\vec{\sigma}\times\vec{\nabla}V)\,, \tag{7}$$

where $\vec{\mathrm{P}}$ is the momentum operator. For Bloch functions we may write,[14]

$$\vec{\pi}=\frac{m}{\hbar}\frac{\partial H(\vec{\mathrm{k}})}{\partial\vec{\mathrm{k}}}\,, \tag{8}$$

a differential expression which has proved quite successful in the numerical prediction of photoemission spectra[15] and optical constants.[16] To compute the matrix elements one need only apply the same similarity transformation to $\vec{\pi}$ that was used to diagonalize H:

$$[E_i]=UHU^{-1}\,,(\hbar/m)[\vec{\pi}_{fi}]=U\frac{\partial H}{\partial\vec{\mathrm{k}}}U^{-1}\,. \tag{9}$$

The additional terms given by Eqs. (3) and (5) are

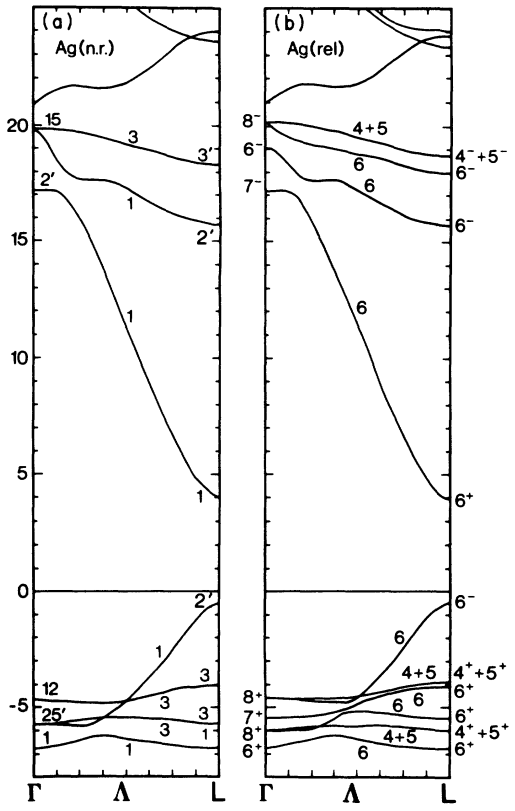

FIG. 2. Comparison for Ag along the $\Gamma\Lambda L$ direction: (a) without and (b) with spin-orbit interactions.

easily differentiable by the k_i and can be straightforwardly incorporated. The magnitude of these terms is much less than that of the rest of the terms arising from the differentiation of the elements of (6). More important is that U, the matrix of eigenfunctions, is properly set up to give the correct eigenvalues upon diagonalization of H. As pointed out by Wang and Callaway,[17] the principal relativistic effects arise not so much through the distinction between $\vec{\pi}$ and $\vec{P}$ but through the relativistic remixing in the eigenfunctions $|i\rangle$ and $|f\rangle$.

B. Numerical results for normal emission from Ag(111)

In photoemission measurements normal to the (111) face, one is confined to that part of the band structure along to the Λ direction, this is shown for Ag in Fig. 2 for both the nonrelativistic and relativistic cases. We will limit our discussion of momentum matrix elements to those which are pertinent to photoemission spectroscopy. In the nonrelativistic version along $\Gamma\Lambda L$, only transitions to bands 7 and 8 need be considered. These have eigenstates which transform as the irreducible representation of Λ_1 of the group C_{3v}. Λ_1 is the symmetrical (or identity) representation and is the only one for which electrons can have a group velocity normal to the surface thereby allowing matching to a running wave in the vacuum. This arises because these two bands have most of the $\vec{G}_{111}$ PW component and correspond to the primary Mahan cones.[18] The selection rules for the nonrelativistic bands are simple: The doubly degenerate Λ_3 bands are coupled to the empty Λ_1 bands only for $\vec{A}\perp\Gamma\Lambda L$ and Λ_1 bands are excited only for $\vec{A}||\Gamma\Lambda L$.

In the relativistic case (double group—Elliott notations[13]) all Λ_1 bands become Λ_6 bands, but the Λ_3 bands split into doubly degenerate (relativistic sense: two spin states) Λ_6 and time-reversal degenerate $\Lambda_4+\Lambda_5$ states (one spin state each). The selection rules are relaxed somewhat: For $\vec{A}\perp\Gamma\Lambda L$, all transitions to Λ_6 states are allowed, but for $\vec{A}||\Gamma\Lambda L$, only the optical transition Λ_6 to Λ_6 is allowed.

Our numerical results for the momentum matrix elements are displayed in Figs. 3–7. Figures 3 and 4 address the parallel polarization case $\vec{A}||\Gamma\Lambda L$ where the electromagnetic vector potential $\vec{A}$ lies along the [111] direction. Figures 5–7 address the case of perpendicular polarization $\vec{A}\perp\Gamma\Lambda L$. In these figures we compare and contrast the nonrelativistic and relativistic cases. In the nomenclature adopted here, $|\Lambda_x\rangle_i^m$ and $|\Lambda_x\rangle_f^n$ denote, respectively, initial and final states. x is the appropriate group represen-

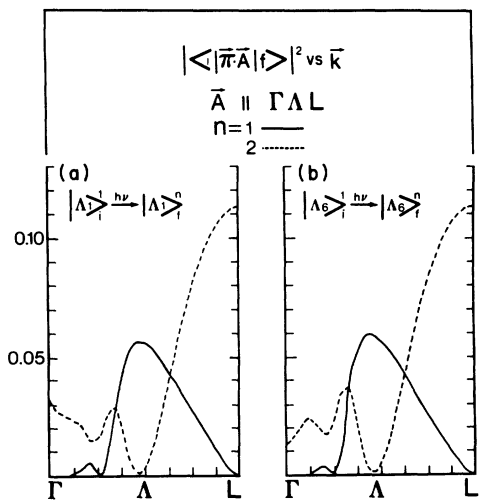

FIG. 3. Numerical results for momentum matrix elements $|\pi_{fi}|^2$ in parallel polarization $\vec{A}||\Gamma\Lambda L$: (a) initial state $|i\rangle$ in the lowest Λ_1 band (nonrelativistic case); (b) initial state $|i\rangle$ in the corresponding lowest Λ_6 of the relativistic case. Solid curves correspond to the final state being in the first unoccupied band $|\Lambda_1\rangle_f^1$ (nonrelativistic) or $|\Lambda_6\rangle_f^1$ (relativistic); dashed curves correspond to the final state being in the second unoccupied band $|\Lambda_1\rangle_f^2$ or $|\Lambda_6\rangle_f^2$.

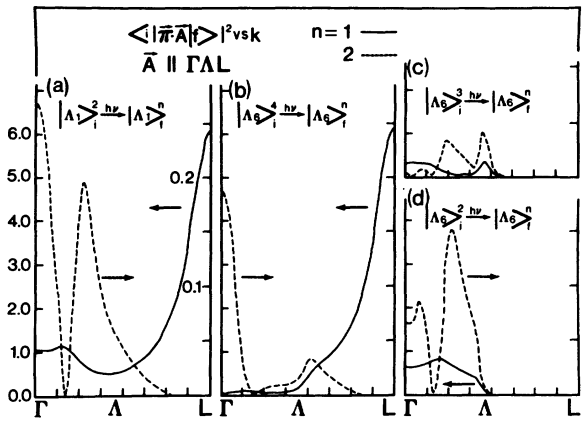

FIG. 4. Numerical results for $|\pi_{fi}|^2$ in parallel polarization $\vec{A}||\Gamma\Lambda L$: (a) initial state $|i\rangle$ in the second occupied Λ_1 band (nonrelativistic case); (b), (c), and (d) initial state $|i\rangle$ in the fourth, third, and second Λ_6 bands, respectively (corresponding relativistic cases). Solid and dashed curves correspond to two final-state bands as in Fig. 3.

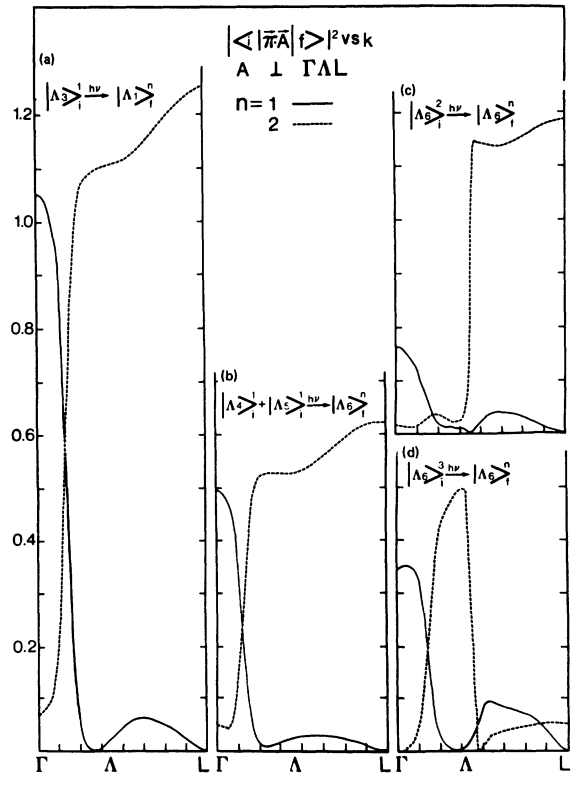

FIG. 5. Numerical results for $|\pi_{fi}|^2$ in perpendicular polarization $\vec{A}\perp\Gamma\Lambda L$: (a) initial state $|i\rangle$ in the lower Λ_3 band (nonrelativistic case); (b) initial state $|i\rangle$ in the $\Lambda_4+\Lambda_5$ band (relativistic case); (c) and (d) initial state $|i\rangle$ in the second and third Λ_6 bands, respectively (relativistic case). Solid and dashed curves correspond to two final-state bands as in Fig. 3.

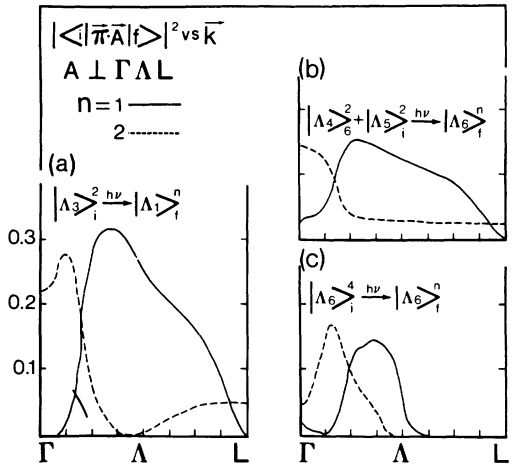

FIG. 6. Numerical results for $|\pi_{fi}|^2$ in perpendicular polarization $\vec{A}\perp\Gamma\Lambda L$: (a) initial state $|i\rangle$ in the second filled Λ_3 band (nonrelativistic case); (b) and (c) initial state $|i\rangle$ in the second $\Lambda_4+\Lambda_5$ band and fourth Λ_6 band, respectively (corresponding relativistic cases). Solid and dashed curves correspond to two final-state bands as in Fig. 3.

tation subscript. Where there is more than one state with representation Λ_x, the superscript m or n distinguishes them in increasing order of energy. We consider only two final-state bands ($n=1,2$). These are the two lowest unoccupied Λ_1 symmetry bands

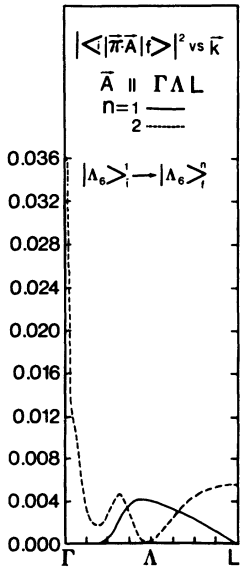

FIG. 7. Numerical results for $|\pi_{fi}|^2$ in perpendicular polarization $\vec{A}\perp\Gamma\Lambda L$ in the relativistic case for transitions from the lowest filled Λ_6 band. Solid and dashed curves correspond to final states in the lowest two unfilled Λ_6 bands. In the nonrelativistic case, transitions from this lowest band are totally symmetry forbidden in perpendicular polarization.

in a nonrelativistic case (designated by the states $|\Lambda_1\rangle_f^1$ and $|\Lambda_1\rangle_f^2$), and these correspond in the relativistic situation to the two lowest unoccupied Λ_6 symmetry bands (designated $|\Lambda_6\rangle_f^1$ and $|\Lambda_6\rangle_f^2$). In Figs. 3–7 the values of $|\vec{\pi}_{fi}\cdot\vec{A}|^2$ are shown as full curves for final states $|\Lambda_1\rangle_f^1$ or $|\Lambda_6\rangle_f^1$ and as dashed curves for $|\Lambda_1\rangle_f^2$ or $|\Lambda_6\rangle_f^2$.

In Fig. 3(a) we show the matrix elements for $\vec{A}||\Gamma\Lambda L$ for the lowest Λ_1 band to the two final Λ_1 bands, and in Fig. 3(b) we show the corresponding relativistic case of Λ_6 to Λ_6 transitions. These are largely the same, differing mainly near Γ where part of the Λ_1 character of what was band 8 has been transferred to band 9 (not shown).

In Fig. 4 we show a similar comparison for the second filled (i.e., higher energy) Λ_1 band to the same two final-state bands. It is important to note that this Λ_1 band crosses the two (initial) Λ_3 bands. On introducing relativistic interactions, each Λ_3 becomes separate Λ_6 and $\Lambda_4+\Lambda_5$ bands. The Λ_6 band arising from the Λ_1 band now hybridizes with the two new Λ_6 bands derived from the Λ_3 bands. Thus there is additional s-d hybridization in this direction in the Brillouin zone. Evidently, this hybridization is weak since the new gaps are small, but we must consider three initial states where formerly there was only one. In Fig. 4(b) we show the matrix elements for transitions from the fourth Λ_6 band to the two final bands. Upon moving from L to the midpoint of the line $\Gamma\Lambda L$, we see that the matrix element is mostly unchanged. Along the remainder of the line the matrix elements formerly associated with Λ_1 have been transferred to the two closest Λ_6 bands. In Figs. 4(c) and 4(d) we show the same transitions from the third and second Λ_6 bands, and this seems to account for most of the matrix elements missing from the fourth initial Λ_6 band.

For the case of $\vec{A}\perp\Gamma\Lambda L$, all transitions are allowed to Λ_6 final states. In Fig. 5(a) we show the results of transitions from the lower Λ_3 band to the final Λ_1 bands. To account for most of the Λ_3 transition strength, we need to consider the lower $\Lambda_4+\Lambda_5$ band and, because of the "no-crossing rule," the second and third Λ_6 bands. Inspection of Figs. 5(b)–5(d) shows at once how the symmetry selection rules are relaxed upon converting to relativistic bands: The transition strength of the nonrelativistic Λ_3 band is divided approximately equally between the relativistic bands of differing symmetries.

Matrix elements for the transitions from the upper initial Λ_3 states are shown in Fig. 6(a). The same for the spin-orbit split bands is shown in Figs. 6(b) and 6(c). The portion of matrix elements for $\Lambda_3^{(2)}$ (initial)$\rightarrow\Lambda_1^{(1),(2)}$ (final) not found in Figs. 6(b) and 6(c) may be found in Fig. 5(b).

There is one more allowed transition to a final Λ_6 state, namely from $|\Lambda_6\rangle_i^1$. The comparable case $|\Lambda_1\rangle_i^1$ is not allowed for $\vec{A}\perp\Lambda\Gamma L$ but is now allowed because of the relaxation of the selection rule. We show this as Fig. 7. The matrix elements are rather small. (Note the change in vertical scale compared with the other figures.) Except near Γ, a region which can be discounted because of low photoelectron escape probability, $|\pi_{fi}|^2$ is generally less than 0.006 in our units.

C. Discussion

The examples of matrix elements presented in Secs. III A and III B allow us to make some generalizations in relation to relativistic and nonrelativistic bands and matrix elements. Firstly, the sum of the squares of the matrix elements for any nonrelativistic optical transition is not very much different than the similar quantity for the composite matrix elements of the appropriate relativistic bands. This is to say that spin-orbit and any other relativistic effects neither add nor subtract much from ordinary matrix elements; rather, they rearrange the bands and redistribute the matrix elements. The matrix element strength of the Λ_3 transitions for $\vec{A}\perp\Gamma\Lambda L$, for example, was approximately evenly distributed among the resulting $\Lambda_4+\Lambda_5$ and Λ_6 transitions in the relativistic case.

One thing to note is that relaxation of a selection rule in going from a nonrelativistic to a relativistic set of bands does not mean that a transition will become strong once it is allowed. On the contrary, if the bands in question are essentially unchanged—i.e., not split off from formerly degenerate bands or hybridized through the relativistic interaction—the matrix elements are still virtually zero. For example, in Figs. 4(c) and 4(d) the half of Λ_6 symmetry lines closest to L were contributed by Λ_3 states. The selection rule states that no transition is allowed, $\Lambda_3\rightarrow\Lambda_1$, for $\vec{A}||\Gamma\Lambda L$, but that $\Lambda_6\rightarrow\Lambda_6$ is allowed. But for all practical purposes, the matrix elements to the Λ_6 final bands for the two Λ_6 initial states which arose from the two Λ_3 initial states nonrelativistically are zero. Similarly, the matrix element for $\vec{A}\perp\Gamma\Lambda L$, $\Lambda_1\rightarrow\Lambda_1$ is strictly zero. The transition $\Lambda_6\rightarrow\Lambda_6$ for the same polarization is allowed, and the matrix element for such transitions from the lowest Λ_6 band are nonzero in general, but are very weak (Fig. 7). Further, transitions for the conduction band (fourth Λ_6 band in the energy range -4–0 eV) are allowed for $\vec{A}\perp\Gamma\Lambda L$, but it is explicitly shown in the appropriate part of the zone of Fig. 6(c) that there is no matrix element to support the transitions.

Borstel *et al.*[6] have discussed the need for using double-group selection rules in materials where rela-

tivistic effects are important. Furthermore, they argue that the lower symmetry associated with relativistic selection rules will permit transitions forbidden in the nonrelativistic case, and the strength of these transitions could be quite appreciable *even in circumstances where the spin-orbit splitting is not resolved.* Our results are in qualitative agreement with this; a good example is the case of the transitions from $|\Lambda_6\rangle_i^1$, which are forbidden nonrelativistically for the perpendicular polarization $\vec{A}\perp\Gamma\Lambda L$, but are permitted in the relativistic case. Quantitatively speaking, however, this effect and many others are found to be rather small. Large effects occur where two bands approach each other closely (or cross) which were not permitted to interact in the nonrelativistic case. In the spirit of perturbation theory, the extent of wave-function admixture now permitted by relativistic interaction will go as $\xi/(E_1-E_2)$, where E_1 and E_2 are the respective band energies and ξ is the appropriate spin-orbit interaction parameter. Thus the energy range over which relativistic selection rules differ significantly from nonrelativistic selection rules will be comparable with the spin-orbit splitting itself. In contradiction to Ref. 6, we conclude that in cases where the energy resolution is insufficient to detect the spin-orbit splitting, relativistic selection rules can largely be ignored. Note also that the experimental spectra presented by Borstel *et al.* to support their argument were taken several degrees away from normal emission. This itself brings about a lowering of symmetry and is probably sufficient to explain the additional peaks they observe.

D. Contact with experiment

Wehner *et al.*[19] have published synchrotron-radiation-derived normal-emission data on Ag(111). It is not our purpose here to analyze fully their data in terms of our results, but one point in their discussion will illustrate the ease with which matrix elements may be applied to experimental results. In their normal emission data, for $\hbar\omega=22$ eV, transitions from band 4 become the dominant feature in the spectrum. This was attributed to transitions to band 7 near Γ where band 7 is quite flat. The matrix elements for this transition are to be found in Figs. 5(d) and 4(c). Note in particular that in Fig. 5(d) the matrix element becomes strong only near Γ where band 7 is quite flat. [The same thing happens in Fig. 4(c) but appears less dramatic because of the larger scale in the figure. The magnitudes of the two differently polarized matrix elements are about the same.] The matrix element gets large just at the point where the escape probability transfers to band 8. In our bands the transition energy is 22.6 eV at that point. Thus our bands and momentum matrix elements are able to explain quantitatively an already published experimental result, and to confirm the identifications made. Further quantitative comparisons between theory and angle-resolved photoemission experiment will be made in a subsequent paper[7] of this series.

ACKNOWLEDGMENTS

We thank Professor Z. Hurych for his continuing encouragement. This work was supported in part by the National Science Foundation under Grant No. DMR-81-08302.

APPENDIX: SYMMETRIZING FACTORS

Each PW of the interpolation scheme has associated with it a symmetrizing factor whose purpose is to compensate for the use of a truncated basis set. (See Refs. 2 and 3.) These were not described in Ref. 5, but their inclusion is essential if one wishes to avoid the spurious removal of degeneracies due to incompleteness of the basis set. They are especially important in the present context where we are concerned with symmetry selection rules in optical transitions. In the work of this paper, and that of Refs. 5, 7, 15, and 16, the symmetrizing factor F_i associated with plane wave $\vec{k}_i$ was assigned the form:

$$F_i=\begin{cases}1 & \text{if } k_i^2<280\\ 0 & \text{if } k_i^2<355\\ 1-(k_i^2-280)^2/5625, & \text{otherwise}.\end{cases}$$

The units of k_i are such that $\Gamma X=8$ units. The scheme, therefore, retains the fully symmetric sets at Γ, L, X, and W up to and including the PW energy $\alpha k_i^2=256\alpha$. Above this energy the PW's are smoothly "switched off." In some papers we have used the alternative range $225<k_i^2<300$.

---

*Mailing address: Synchrotron Radiation Center, 3725 Schneider Drive, Stoughton, Wisconsin 53589.

[1]E. Dietz and D. E. Eastman, Phys. Rev. Lett. 41, 1674 (1978); R. Courths, V. Bachelier, B. Cord, and S. Hüfner, Solid State Commun. 40, 1059 (1981); M. Pessa, M. Lindroos, H. Asonen, and N. V. Smith, Phys. Rev. B 25, 738 (1982).

[2]N. V. Smith and L. F. Mattheiss, Phys. Rev. B 9, 1341 (1974).

[3]L. Hodges, H. Ehrenreich, and N. D. Lang, Phys. Rev.

152, 505 (1966).
[4]F. M. Mueller, Phys. Rev. 153, 659 (1967).
[5]N. V. Smith, Phys. Rev. B 19, 5019 (1979).
[6]G. Borstel, M. Neumann, and M. Wöhlecke, Phys. Rev. B 23, 3123 (1981); also see A. Goldmann, D. Westphal, and R. Courths, *ibid.* 25, 2000 (1982); G. Borstel, H. Przybylski, M. Newmann, and M. Wöhlecke, *ibid.* 25, 2006 (1982).
[7]R. L. Benbow, M. R. Thüler, Z. Hurych, and N. V. Smith (unpublished).
[8]N. V. Smith, Phys. Rev. B 9, 1365 (1974).
[9]N. E. Christensen, Phys. Status Solidi B 54, 551 (1972).
[10]N. E. Christensen and B. O. Seraphin, Phys. Rev. B 4, 3321 (1971).
[11]M. L. Cohen and V. Heine, in *Solid State Physics,* edited by F. Seitz, D. Turnbull, and H. Ehrenreich (Academic, New York, 1970), Vol. 24, p. 72.
[12]E. Abate and M. Asdente, Phys. Rev. 140, A1013 (1965); see also J. Friedel, P. Lenglart, and G. Leman, J. Phys. Chem. Solids 25, 781 (1964).
[13]R. J. Elliott, Phys. Rev. 96, 280 (1954).
[14]E. I. Blount, in *Solid State Physics,* edited by F. Seitz and D. Turnbull (Academic, New York, 1970), Vol. 13, p. 305.
[15]N. V. Smith, R. L. Benbow, and Z. Hurych, Phys. Rev. B 21, 4331 (1980).
[16]R. Lässer, N. V. Smith, and R. L. Benbow, Phys. Rev. B 24, 1895 (1981); *ibid.* 25, 1910 (1981); 25, 806 (1982); N. V. Smith, R. Lässer, and S. Chiang, *ibid.* 25, 793 (1982).
[17]C. S. Wang and J. Callaway, Phys. Rev. B 9, 4897 (1974).
[18]G. D. Mahan, Phys. Rev. B 2, 4334 (1970).
[19]P. S. Wehner, R. S. Williams, S. D. Kevan, D. Denley, and D. A. Shirley, Phys. Rev. B 19, 6164 (1979).